

## Infrared spectroscopic investigation of higher diamondoids

Jos Oomens<sup>a,\*</sup>, Nick Polfer<sup>a</sup>, Olivier Pirali<sup>a</sup>, Yuko Ueno<sup>b,c</sup>, Roha Maboudian<sup>b</sup>,  
Paul W. May<sup>d</sup>, Jacob Filik<sup>d</sup>, Jeremy E. Dahl<sup>e</sup>, Shenggao Liu<sup>e</sup>, Robert M.K. Carlson<sup>e</sup>

<sup>a</sup> FOM Institute for Plasma Physics “Rijnhuizen”, Edisonbaan 14, 3439 MN Nieuwegein, The Netherlands

<sup>b</sup> Department of Chemical Engineering, University of California Berkeley, Berkeley, CA 94720, USA

<sup>c</sup> NTT Microsystem Integration Laboratories, Atsugi, Kanagawa 243-0198, Japan

<sup>d</sup> School of Chemistry, University of Bristol, Bristol BS8 1TS, UK

<sup>e</sup> Molecular Diamond Technology, Chevron Technology Ventures, Richmond, CA 94802, USA

Received 11 April 2006

Available online 5 May 2006

### Abstract

Attenuated total reflection Fourier transform infrared spectra are recorded for a number of diamond molecules (or higher diamondoids) in the spectral range between 650 and 3000  $\text{cm}^{-1}$ . Molecules studied are diamantane, triamantane, [121]tetramantane, [123]tetramantane, [1(2,3)4]pentamantane, [12(3)4]pentamantane, 3-methyl-[1(2,3)4]pentamantane, and [12312]hexamantane (cyclohexamantane). Spectral trends are clearly recognized throughout the spectra revealing the general fingerprint of this class of molecules. In general, the spectra show good agreement with density functional theory calculations at the B3LYP/D95(d,p) level of theory.

© 2006 Elsevier Inc. All rights reserved.

**Keywords:** Diamondoids; Infrared; Spectroscopy

### 1. Introduction

Diamondoid molecules consist of a diamond-like carbon cage, where all carbon atoms are  $\text{sp}^3$  hybridised, and dangling bonds at the edges of the systems are terminated with hydrogen atoms. The smallest member of the family, adamantane ( $\text{C}_{10}\text{H}_{16}$ ) is made up of the central cage of a single diamond unit cell and was first synthesized by carbocation equilibration in 1957 by von Rague Schleyer [1]. The next members of the family are diamantane and triamantane possessing two and three diamond cages, respectively. For higher diamondoids, starting with tetramantane (four cages), structural isomers can be formed.

Diamondoids show remarkable rigidity, strength, and thermodynamic stability, as well as interesting electronic properties [2], which may be of use in chemical, polymer, and pharmaceutical applications, as well as in nanotechnology.

Moreover, there has been substantial interest in the spectroscopic properties of this class of molecules from an astrophysical view-point. Not only have nanometer-sized ‘diamond-like’ molecules been found in meteorites [3], the occurrence of these compounds as isolated gas-phase molecules in the interstellar medium, has also been suggested, based on the observation of infrared absorption [4] and emission [5,6] bands around 3.5  $\mu\text{m}$  ( $2880 \text{ cm}^{-1}$ ) in the spectra of protostars as well as the post-AGB object HR 4049 [6]. This band has been assigned to the tertiary  $\text{sp}^3$  carbon (i.e., carbon bound to three carbon atoms) C–H stretching mode [7], but other explanations have also been put forward [8,9]. Further evidence for the existence of interstellar diamondoid molecules could be obtained by comparing the complete vibrational spectra of such diamondoids with astronomical data [10].

Although the very smallest members of the diamondoid family can now be readily synthesized, this is not the case for species larger than triamantane. Hence, in spite of the wide interest in diamondoids, relatively few studies have been reported on the characterization of these molecules.

\* Corresponding author. Fax: +31 30 603 12 04.

E-mail address: [joso@huygens.rijnh.nl](mailto:joso@huygens.rijnh.nl) (J. Oomens).

A recent breakthrough in diamondoid research was the discovery that higher diamondoids can be isolated from petroleum, which was shown for species up to the size undecamantane (11 cages) [11]. As a result, various analytical techniques including GC/MS and NMR have been applied to identify and characterize these novel species [12].

From a spectroscopic point of view, only Raman spectra of a selection of diamondoids with a size ranging from adamantane to [121321]heptamantane have been published very recently [13]. In addition, theoretical methods have been applied to predict the vibrational spectra of some of these molecules. An extensive computational study of adamantane and some of its ionic and dehydrogenated

radical species was reported by Yan et al. [14]. For the adamantyl closed-shell cation, an experimental infrared spectrum was also obtained [15]. The Raman spectrum of crystalline cyclohexamantane was interpreted with density functional theory (DFT) calculations by Richardson et al. [16]. An infrared spectroscopic study on deposited diamondoid nanoparticles (5–350 nm in size) focusing on the 3  $\mu\text{m}$  spectral range was successfully interpreted with DFT computations on individual molecular diamondoid structures, giving insight into the size dependence of the spectra [17].

To our knowledge, no infrared spectra have to date been reported for individual higher diamondoid molecules. Moreover, no direct comparison between theoretical and experimental spectra for these molecules has been reported. In this contribution, we present the first infrared spectra for a number of higher diamondoids, and present an analysis based on DFT computations of the vibrational spectra. The systems studied are diamantane, triamantane, [121]tetramantane, [123]tetramantane, [1(2,3)4]pentamantane, [12(3)4]pentamantane, and [12312]hexamantane (cyclohexamantane), which are shown in Fig. 1. (Note that we follow the nomenclature introduced in ref. [18].) In addition, we present the infrared spectrum for the [1(2,3)4]pentamantane molecule methylated at the position of the arrow in Fig. 1 (3-methyl-[1(2,3)4]pentamantane).

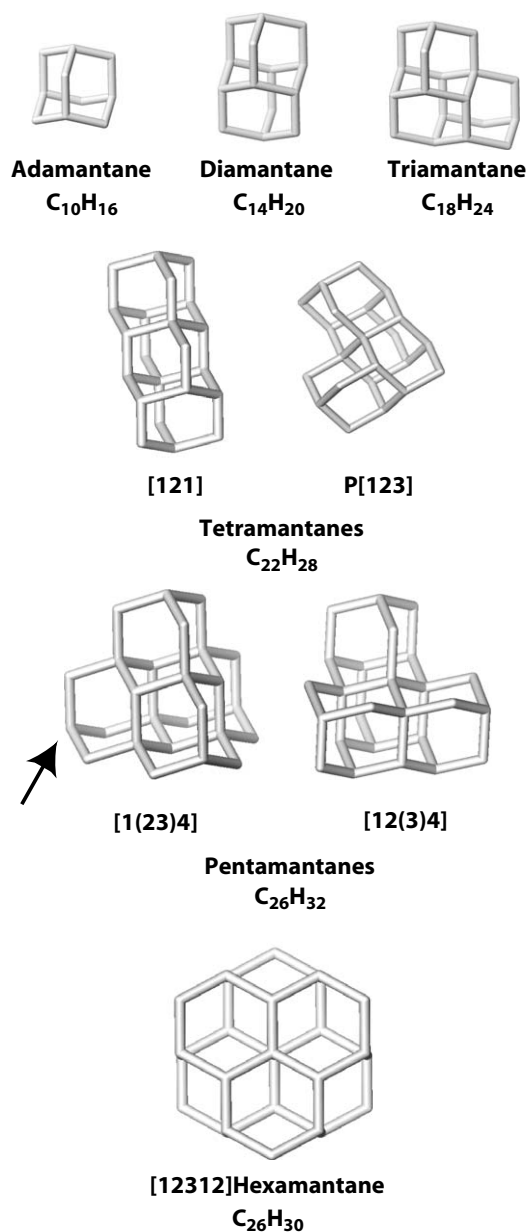


Fig. 1. Higher diamondoid structures considered in this work. Hydrogen atoms have been omitted for clarity; all structures are fully saturated. The smallest member of the family, adamantane, is shown for comparison. The arrow indicates the carbon atom where by the substitution of a hydrogen atom for a methyl group, the 3-methyl-[1(2,3)4]pentamantane is formed.

## 2. Methods

### 2.1. Experimental

Higher diamondoid species (size going up to undecamantane) have been isolated from petroleum oil by vacuum distillation, high-temperature pyrolytic destruction of non-diamondoid species combined with chromatographic techniques [11]. The size and shape separations are performed using high performance liquid chromatography in ultrahigh purity. The molecules studied here are neutrals, fully  $\text{sp}^3$  hybridized molecules with completely hydrogenated surfaces plus one mono-methylated species.

The attenuated total reflection Fourier transform infrared (ATR-FTIR) spectra of the diamondoid molecules were recorded with the use of a Thermo Nicolet Avatar 370 FT-IR spectrometer and an ATR accessory with a ZnSe ATR crystal. The spectra of [12(3)4]pentamantane and 3-methyl-[1(2,3)4]pentamantane were recorded in Bristol (UK) at slightly higher resolution, using a Perkin-Elmer ‘Spectrum One’ FTIR spectrometer. The higher resolution was required to better resolve the bands in the congested spectra of these molecules. All spectra are obtained from pure, powdered diamondoid samples, and measurements were performed at room temperature. The intensity of the ATR absorbance spectra are corrected for the penetration depth of the evanescent wave, which is proportional to the wavelength.

One can notice that two enantiomers (P and M) exist for the molecule [123]tetramantane. Since the light source used

to obtain the ATR-FTIR spectra is not polarized, the spectrum recorded is not dependent on the enantiomer studied. The structure of the P[123]tetramantane is given in the Fig. 1, but the recorded spectrum corresponds to a racemic mixture of the P and M enantiomers.

## 2.2. Computational

Geometry optimization and computation of the harmonic vibrational frequencies were performed using the Becke3LYP hybrid density functional [19] and Dunning's double zeta basis set with polarization functions, D95(d,p). This method has been shown to give reliable results for numerous organic compounds, such as a large variety of polycyclic aromatic hydrocarbons [20]. The computations are carried out at an IBM cluster1600 system located at the SARA Supercomputer center in Amsterdam using the Gaussian98 program package [21].

The high symmetry of many of the systems was conveniently used to reduce the computational cost of the calcu-

lations. All calculations converged and yielded no negative frequencies. For comparison with the experimental spectra, the calculated spectra have been convoluted with a  $5\text{ cm}^{-1}$  FWHM Gaussian line profile (except for the spectra recorded at higher resolution in Bristol, where a  $2.5\text{ cm}^{-1}$  FWHM Gaussian convolution was used in the mid-infrared range).

Due to the generally substantial differences in anharmonicity for the CH stretching modes in the  $3\text{ }\mu\text{m}$  spectral range as compared to the modes in the mid-infrared range, empirical scaling factors are commonly determined for the two spectral ranges separately. In the  $3\text{ }\mu\text{m}$  region, a scaling of the computed frequencies was applied so that the most intense peak matches exactly. In the mid-infrared range, the scaling was (arbitrarily) chosen such that the strong peak occurring around  $1050\text{--}1150\text{ cm}^{-1}$  shows exact agreement. Thus, average scaling factors of 0.986 and 0.947 are found for the mid-infrared and CH stretching regions (see Table 1), respectively, which appears to be nicely in accord with the overall value of 0.961 reported for the B3LYP functional [22]. Moreover, the  $3\text{ }\mu\text{m}$  scaling factor of 0.947 is very close to that of 0.946 reported by Chen et al. [17] for computed harmonic frequencies of large diamondoids using the same functional but with the 6-31G(d) basis set.

## 3. Results and discussion

The spectra are displayed in Figs. 2–9, compared “back-to-back” with the scaled computed spectra. As expected, the spectra of the more symmetric species are much simplified relative to those of the less symmetric ones, even if they are bigger in size; a striking example

Table 1  
Empirical scaling factors for DFT computed frequencies

	Formula	Sym	Frequency scaling	
			Mid-IR	$3\text{ }\mu\text{m}$
Diamantane	$\text{C}_{14}\text{H}_{20}$	$\text{D}_{3d}$	0.9916	0.949
Triamantane	$\text{C}_{18}\text{H}_{24}$	$\text{C}_{2v}$	0.986	0.947
[121]Tetramantane	$\text{C}_{22}\text{H}_{28}$	$\text{C}_{2h}$	0.986	0.947
[123]Tetramantane	$\text{C}_{22}\text{H}_{28}$	$\text{C}_2$	0.988	0.948
[1(2,3)4]Pentamantane	$\text{C}_{26}\text{H}_{32}$	$\text{T}_d$	0.975	0.947
[12(3)4]Pentamantane	$\text{C}_{26}\text{H}_{32}$	$\text{C}_s$	0.985	0.941
[12312]Hexamantane	$\text{C}_{26}\text{H}_{30}$	$\text{D}_{3d}$	0.990	0.948
3-Methyl-[1(2,3)4]pentamantane	$\text{C}_{27}\text{H}_{34}$	$\text{C}_{3v}$	0.976	0.945

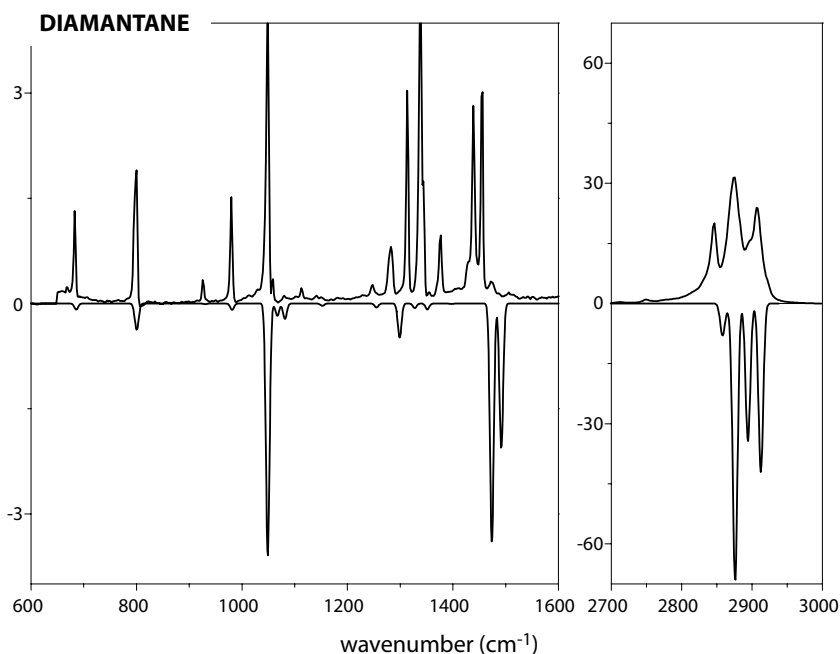


Fig. 2. Infrared spectrum of diamantane.

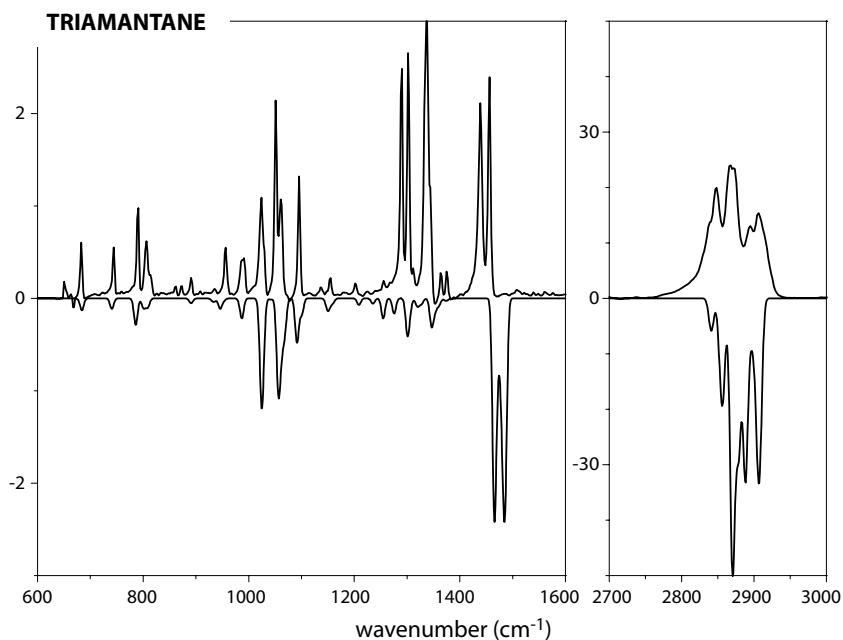


Fig. 3. Infrared spectrum of triamantane.

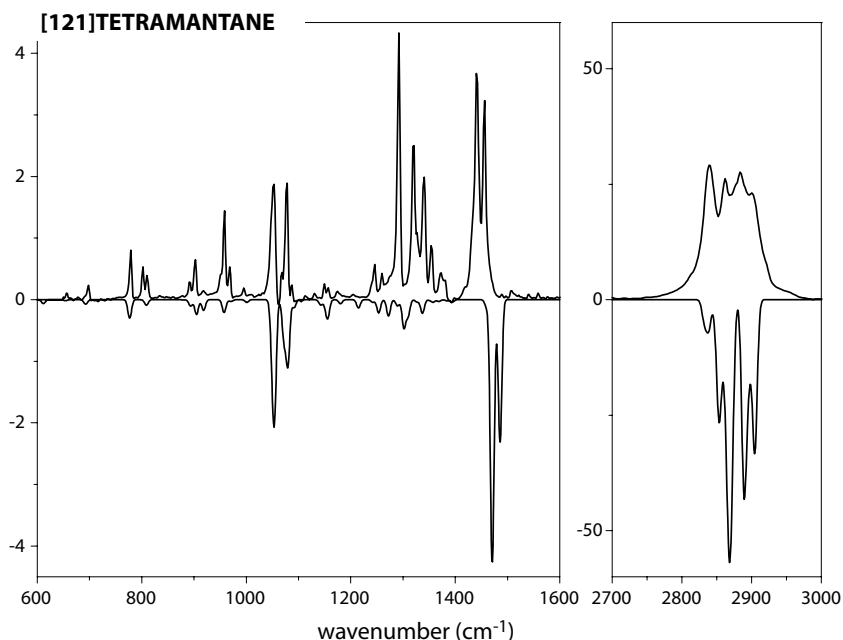


Fig. 4. Infrared spectrum of [121]tetramantane.

is observed by comparing the spectra of [123]tetramantane ( $C_2$ ) with those of [1(2,3)4]pentamantane ( $T_d$ ) or [12312]hexamantane ( $D_{3d}$ ). On the other hand, one can also notice that the spectra of two different molecules belonging to the same symmetry group can be quite different. Compare for example the spectra of adamantane (see ref. [23]) and [1(2,3)4]pentamantane (both  $T_d$  symmetry) or diamantane and [12312]hexamantane (both  $D_{3d}$  symmetry). However, despite the dense spectrum for the lower symmetry species, the experimental-

versus-theoretical match in the mid-infrared frequency range is usually acceptable. For instance, the spectra of [123]tetramantane (Fig. 5) and [12(3)4]pentamantane (Fig. 7), recorded at higher resolution because of the highly congested mid-infrared spectrum, show good agreement with theory.

At this point we could discuss the spectrum of each molecule individually, however, we have chosen to discuss the cyclohexamantane spectrum in somewhat more detail and then give a more general discussion of the spectra of the

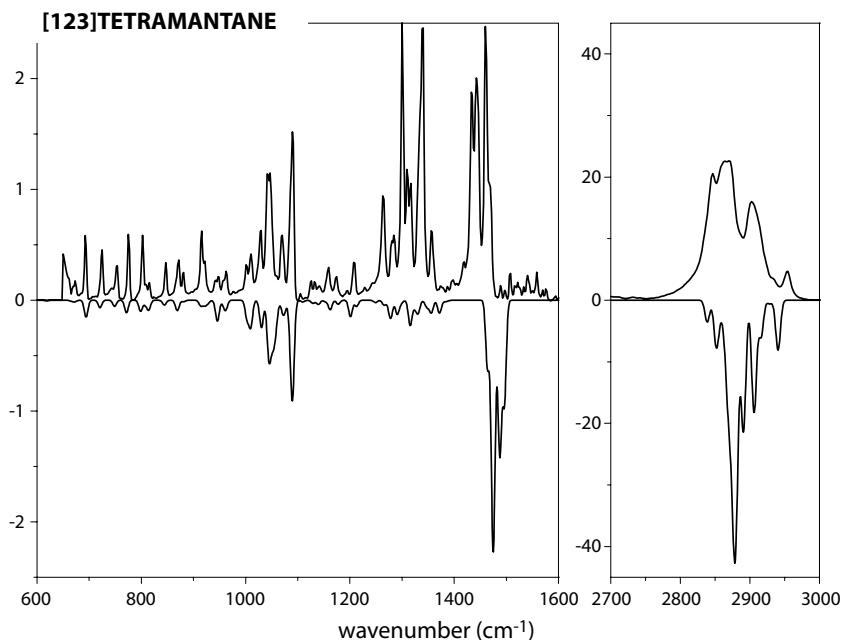


Fig. 5. Infrared spectrum of [123]tetramantane.

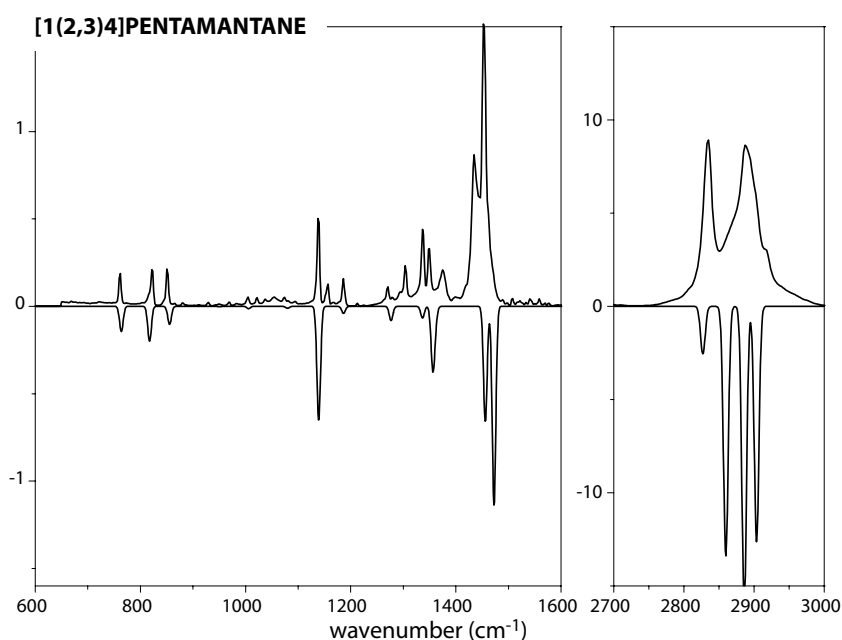


Fig. 6. Infrared spectrum of [1(2,3)4]pentamantane.

remaining molecules. Experimental peak listings and computed optimized structures for all molecules can be found in the [Supplementary material](#). The choice for hexamantane is not completely arbitrary since due to the high symmetry of the molecule, it represents a relatively simple and clean spectrum. Moreover, this particular higher diamondoid seems to have received more attention than others recently [12,16]. It is the largest species in the series investigated here. Finally, we briefly investigate the effect of methylation on the spectrum by discussing the spectrum

of 3-methyl-[1(2,3)4]pentamantane in somewhat more detail.

### 3.1. IR spectrum of cyclohexamantane

[12312]Hexamantane or cyclohexamantane belongs to the  $D_{3d}$  symmetry group and this high symmetry simplifies the infrared spectrum considerably. Of the 162 vibrational modes, only those of  $A_{2u}$  and  $E_u$  symmetry are infrared allowed. The  $E_u$  modes are doubly degenerate. From the

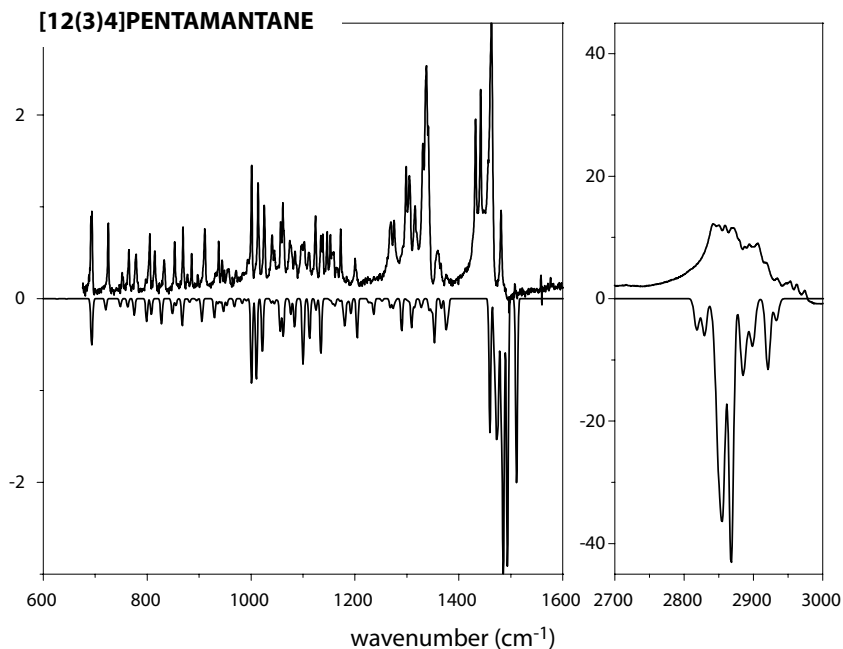


Fig. 7. Infrared spectrum of [12(3)4]pentamantane. The resolution of the calculated spectrum is  $2.5 \text{ cm}^{-1}$ .

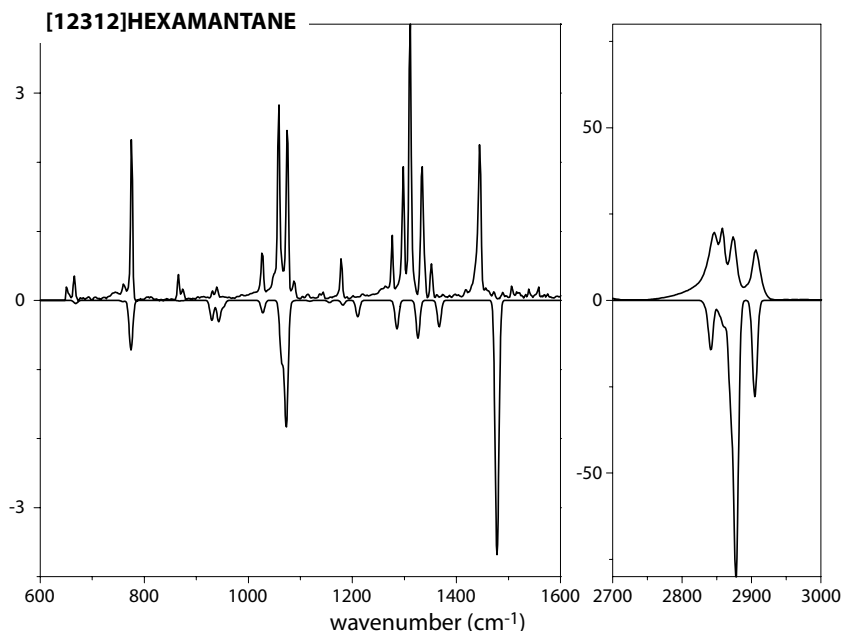


Fig. 8. Infrared spectrum of [12312]hexamantane.

comparison of the experimental and theoretical spectra shown in Fig. 8, it is quite straightforward to obtain an assignment for the majority of the bands. Some difficulties are encountered in the  $1250\text{--}1400 \text{ cm}^{-1}$  range, where more bands, and with more intensity, are observed than calculated. In the CH stretching range around  $2800\text{--}2900 \text{ cm}^{-1}$ , the proximity of several very intense modes causes severe congestion in the experimental spectrum, which makes a secure assignment very difficult. The proposed assignments are

listed in Table 2, where those in the above mentioned wavenumber ranges should be regarded as tentative at best.

Table 2 shows that using the scaling factors of Table 1 gives a deviation of less than  $5 \text{ cm}^{-1}$  for all bands except for the bands in the  $1250\text{--}1400 \text{ cm}^{-1}$  range. In addition, for the band observed at  $1445 \text{ cm}^{-1}$ , assigned securely as a  $\text{CH}_2$  scissoring mode, the deviation of more than  $20 \text{ cm}^{-1}$  appears to be anomalously large. In fact, two closely spaced scissoring modes are predicted, one of  $E_u$  and one of  $A_{2u}$

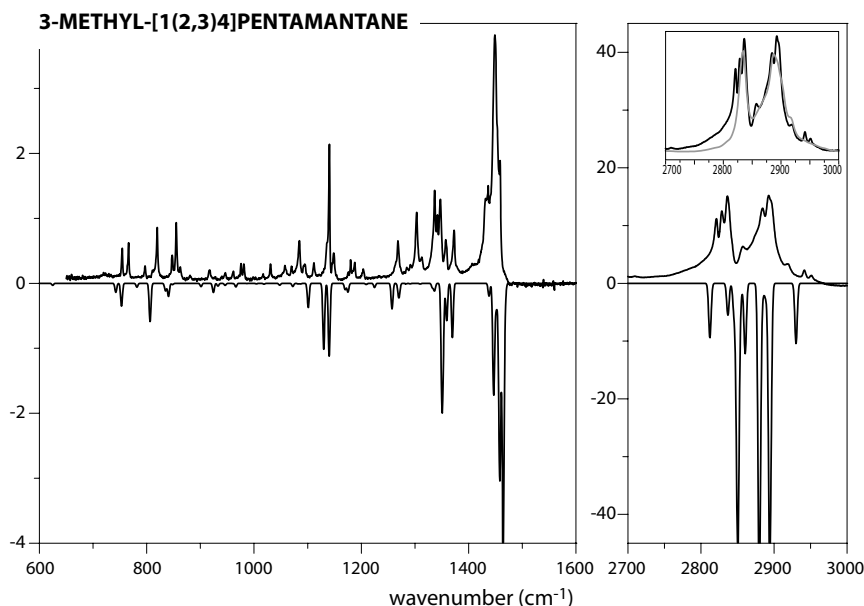


Fig. 9. Infrared spectrum of 3-methyl-[1(2,3)4]pentamantane. A comparison with the 3- $\mu\text{m}$  spectrum of its non-methylated counterpart is shown in the inset.

Table 2  
Infrared active modes of cyclohexamantane, experimental versus calculated

Calc freq ( $\text{cm}^{-1}$ )	Intensity (km/mol)	Sym	Exp freq ( $\text{cm}^{-1}$ )	Description
668.2	0.2	$E_u$	665	Deform
758.9	0.2	$A_{2u}$	760	Deform
774.4	4	$E_u$	775	Deform
867.1	0.1	$A_{2u}$	865	$\text{CH}_2$ rock
873.5	0.02	$E_u$	874	Deform/ $\text{CH}_2$ rock
929.9	2	$E_u$	931	Deform/ $\text{CH}_2$ rock
943.0	2	$E_u$	939	CC str/CH bend
952.1	1	$A_{2u}$	—	CC str/CH bend
1027.9	1	$E_u$	1026	CC str/CH bend
1063.9	4	$E_u$	1058	$\text{CH}_2$ wag/CH bend
1073.0	19	$A_{2u}$	1074	$\text{CH}_2$ rock/CH bend
1084.0	0.1	$E_u$	1088	CH bend
1118.2	0.1	$E_u$	—	$\text{CH}_2$ twist/CH bend
1181.8	0.7	$A_{2u}$	1178	CC str/CH bend
1210.3	1	$E_u$	—	CH bend
1280.8	0.1	$E_u$	1276	CH bend/ $\text{CH}_2$ twist
1285.8	2	$E_u$	1297	CH bend
1326.1	6	$A_{2u}$	1311	CH bend
1366.8	2	$E_u$	1337	CH bend
1368.1	0.3	$A_{2u}$	1352	CH bend
1477.7	13	$E_u$	1445	$\text{CH}_2$ scissor
1478.7	13	$A_{2u}$	—	$\text{CH}_2$ scissor
2834.6	8	$E_u$	—	CH str
2841.5	150	$A_{2u}$	2847	CH str
2853.2	17	$E_u$	—	CH str
2858.5	2	$A_{2u}$	—	CH str
2860.4	36	$E_u$	2858	CH str
2870.1	293	$A_{2u}$	—	CH str
2877.9	418	$E_u$	2874	CH str
2904.4	62	$E_u$	—	CH str
2905.3	176	$A_{2u}$	2906	CH str

character. The experimental band at  $1445\text{ cm}^{-1}$  indeed appears to be somewhat asymmetrically shaped suggesting the presence of two unresolved bands. When the molecule

is viewed along the (100) crystal lattice plane, the modes correspond to asymmetric scissoring of the  $\text{CH}_2$  moieties on diagonally opposing corners of the molecule.

As impressive as the match for the frequencies is, the intensity predictions are not all that excellent. Particularly the relative intensities of the modes in the 1250–1400  $\text{cm}^{-1}$  range are underestimated. Moreover, the intensity ratio between the CH stretching range and the rest of the spectrum is not so well reproduced.

Analogous to for instance olefins and acetylenes, the strongest CH stretching bands roughly correspond to collective asymmetric stretching modes, though now along one of the crystal lattice planes. For instance in cyclohexamantane, the band calculated at 2877.9  $\text{cm}^{-1}$  corresponds to the asymmetric CH stretching band in the (110) lattice plane, the band at 2905.3  $\text{cm}^{-1}$  oscillates asymmetrically in the (111) plane, and the 2870.1 and 2841.5  $\text{cm}^{-1}$  bands in the (100) lattice plane.

### 3.2. General discussion of diamondoid spectra

Upon global inspection of all spectra, one clearly observes large similarities between them. Many parallels with the cyclohexamantane spectrum can be observed, although the lower symmetry of most other species yield a richer vibrational pattern. The general appearance of the spectra could be considered as the spectral fingerprint of the diamondoid class of molecules. Inspecting the spectra more closely, four distinct groups of bands can be recognized in all diamondoid spectra. Visualization of the calculated vibrational displacements allows one to roughly assign a general mode description pertinent to the four groups (see Table 3).

The modes around 2900  $\text{cm}^{-1}$  (Group A) are of course the CH stretching modes. Due to the very strong and overlapping bands and the broader line widths in the 3  $\mu\text{m}$  range, it is harder to recognize the quality of the match. In some cases, it appears that the experimental bands are more widely spaced than their computed counterparts. A possible explanation could be strong anharmonic interactions between closely spaced modes of equal symmetry, which all have very similar CH stretching character.

A very recognizable group of modes in all spectra, mostly appearing as a doublet around 1450  $\text{cm}^{-1}$  is due to two or more  $\text{CH}_2$  scissoring modes. These bands are clearly identifiable throughout the spectra, mostly appearing as a doublet. In [123]tetramantane, the low symmetry causes further splitting into about four bands. In [12312]hexamantane, where only a single band is observed, the computation predicts three bands with non-vanishing intensity

within 1  $\text{cm}^{-1}$ . In all cases the bands are well reproduced by theory, except for a consistent blue shift of the calculated frequencies of around 35  $\text{cm}^{-1}$ . A slightly smaller scaling factor of about 0.966 on average appears to be more appropriate for these modes. Compared to the average scaling factor used for the mid-infrared range of 0.986 (see Table 1) this amounts to a discrepancy of 2 %. Despite this discrepancy, the assignment appears to be fairly secure on account of the consistency of the shift and the recurring pattern of these bands throughout the spectra (see Figs. 2–9).

The bands falling roughly between 1000 and 1400  $\text{cm}^{-1}$  have mostly CH bending and  $\text{CH}_2$  rocking, wagging, and twisting character. Toward the red end of this group, some CC stretching character is found. Finally, in the long wavelength part of the spectra, below 1000  $\text{cm}^{-1}$ , mostly skeletal deformation modes are found and these modes have been classified as belonging to Group D in Table 3. Comparing the bands in Groups C and D to the DFT calculation, a striking observation is the underestimation of their intensities (except some around 1050  $\text{cm}^{-1}$ ) by the DFT calculations. The reason for this discrepancy, that appears to be a general feature in all diamondoid spectra, is at present unclear. A possible influence of the basis set used was investigated for the [121]tetramantane molecule (see Fig. 10). However, the underestimation of intensities in Groups C and D is consistently reproduced upon using basis sets ranging in size from 3-21G to cc-pVDZ.

As to the computed frequencies, one notices in Fig. 10 that the frequency scaling factor becomes closer to unity as the basis set is increased, which is a well-known effect. Interestingly, however, the  $\text{CH}_2$ -scissoring modes (Group B) appear to shift more than the other bands in the spectrum, such that the anomalous scaling factor mentioned for these modes above, is almost completely corrected for when using the cc-pVDZ basis set.

In conclusion, a global inspection of the spectra shows that the match between theoretical and experimental frequencies is reasonable for most of the bands in the mid-infrared range. This does, however, not apply to the relative intensities, which are not so well reproduced. Although intensities were corrected for the wavelength dependency of ATR, there remains a significant discrepancy (a factor of 3 approximatively) between the experimental and computed intensity ratios for the mid-IR versus the 3  $\mu\text{m}$  spectral ranges. Judging from the increased linewidth and the more Lorentzian-like lineshape, it seems that this discrepancy results at least partly from saturation in the 3  $\mu\text{m}$  range. It is, however, also known that while DFT usually provides a good prediction of the frequencies, intensities are not so reliably predicted. In addition, interaction of the molecules with their solid environment may affect the intensities differently for different vibrational modes. In fact, for a number of polyaromatic molecules, Joblin et al. [24] found that the CH stretching modes were attenuated by a factor of 3 in the solid-phase with respect to the gas-phase. Although such an effect would indeed explain

Table 3  
General assignment pertinent to all molecules studied in four distinct spectral ranges

	Region ( $\text{cm}^{-1}$ )	General description
Group A	2900	CH stretch
Group B	1450	$\text{CH}_2$ scissor
Group C	1000–1400	$\text{CH}_2$ rock, wag, twist
Group D	$\leq 1000$	Skeletal deformation

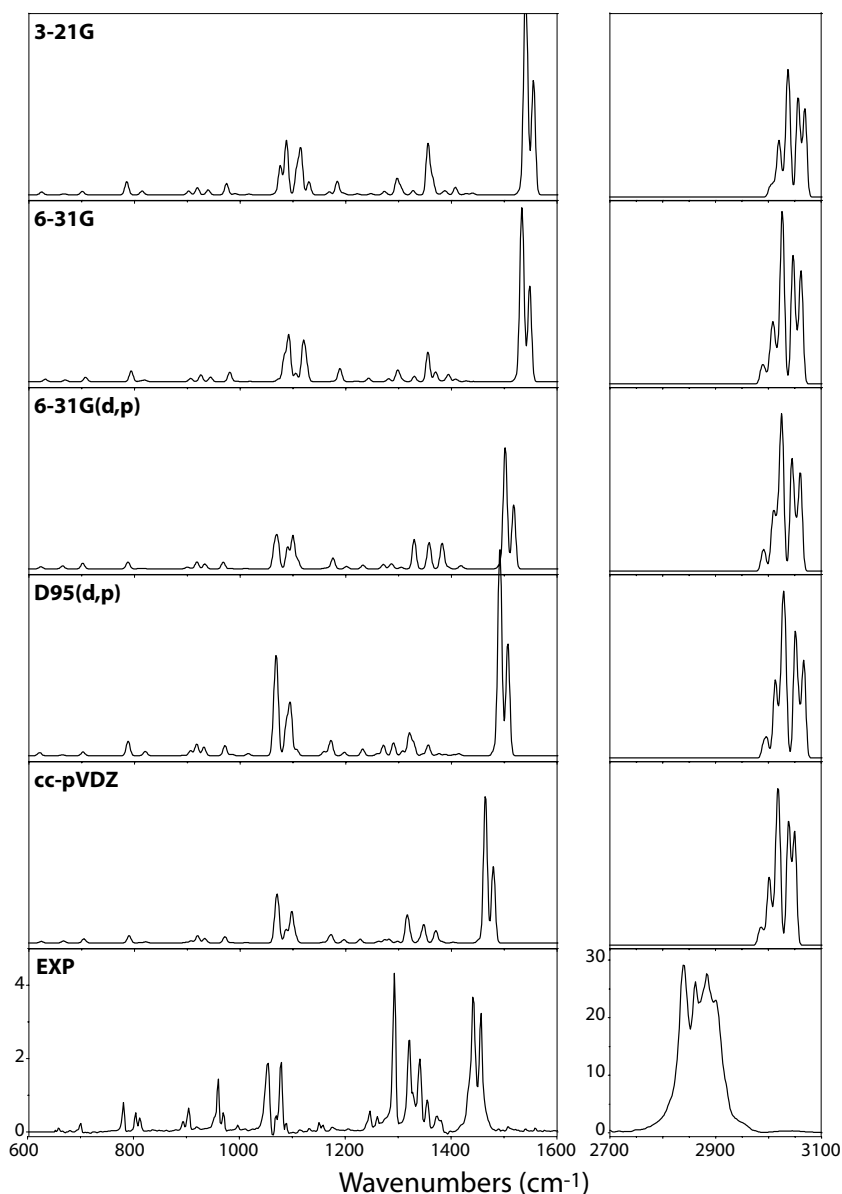


Fig. 10. Infrared spectrum of [121]tetramantane compared to (unscaled) calculated spectra using different basis sets.

here the observed discrepancies, only when gas-phase diamondoid spectra become available can such a conclusion be truly substantiated.

### 3.3. Methyl substitution at the surface of the cage

In addition to the pure diamondoid molecules, the infrared spectrum has been recorded for a methyl substituted diamondoid: 3-methyl-[1(2,3)4]pentamantane (see Fig. 9), where the H atom at the position indicated with an arrow in Fig. 1 is substituted by a CH<sub>3</sub> group (thereby causing a reduction in symmetry from T<sub>d</sub> to C<sub>3v</sub>).

With respect to the general appearance of diamondoid spectra as described above, significant differences are found. In the CH stretching region around 3 μm, the

calculation produces CH stretching modes localized on the methyl group at 2930.1 and 2860.5 cm<sup>-1</sup>, corresponding to the CH<sub>3</sub> stretching modes parallel and perpendicular to the threefold symmetry axis, respectively. These modes can be well observed in the experimental spectrum, particularly when it is compared with the experimental spectrum of the non-methylated [1(2,3)4]pentamantane (see inset in Fig. 9). Though weak, additional bands are observed for the methylated species at 2857 cm<sup>-1</sup> and around 2945 cm<sup>-1</sup> (we cannot explain the observation of what appears to be a doublet at present). At the red end of the CH stretching manifold, there appears to be another additional band at about 2820 cm<sup>-1</sup>, but the calculation indicates that this band is due to the three degenerate CH stretching modes in the (111) lattice plane,

which are red-shifted by about  $10\text{ cm}^{-1}$  in the methylated molecule with respect to the non-methylated one.

In the remainder of the spectrum, it is not so easy to pinpoint the direct influence of the methyl group on the spectrum. Comparison of the spectrum with that of unsubstituted [1(2,3)4]pentamantane (see Fig. 6) clearly shows that additional bands appear, but inspection of the corresponding normal modes indicates that they are due to non-localized modes. It therefore appears that these differences are mainly induced by the reduction of symmetry from  $T_d$  for [1(2,3)4]pentamantane to  $C_{3v}$  for 3-methyl-[1(2,3)4]pentamantane.

Some local modes of the methyl group are computed at  $1369.7\text{ cm}^{-1}$  ( $\text{CH}_3$  umbrella) and  $1457.0\text{ cm}^{-1}$  ( $\text{CH}_3$  scissor), but they are not easily recognized in the experimental spectrum, probably due to overlapping diamondoid bands.

#### 4. Conclusion

We report in this paper the first infrared spectroscopic characterization of several higher diamondoid molecules. These experimental spectra, supported with density functional theory calculations provide the spectroscopic fingerprint for this class of molecules. Among others, this may strengthen a possible detection of this family of compounds in different astrophysical objects, which has thus far been based only on the observation of CH stretching bands around  $2850\text{ cm}^{-1}$ . In general, a good agreement between experiments and DFT computations was found, which allowed us to identify several groups of bands corresponding to certain classes of molecular vibrations. Finally, methyl substitution on the diamondoid cage induced significant changes particularly in the  $3\text{ }\mu\text{m}$  range of the spectrum, which may help to evaluate their astrophysical relevance.

#### Acknowledgments

We gratefully acknowledge the SARA Supercomputer center in Amsterdam, The Netherlands, for providing the CPU time. This work is part of the research program of FOM (Project No. 03PR2218), which is financially supported by the ‘Nederlandse Organisatie voor Wetenschappelijk Onderzoek (NWO)’.

#### Appendix A. Supplementary data

Supplementary material. Optimized structures at the B3LYP/D95(d,p) level for all molecules studied here as well as experimental frequencies.

Supplementary data for this article are available on ScienceDirect ([www.sciencedirect.com](http://www.sciencedirect.com)) and as part of the Ohio State University Molecular Spectroscopy Archives ([http://msa.lib.ohio-state.edu/jmsa\\_hp.htm](http://msa.lib.ohio-state.edu/jmsa_hp.htm)).

#### References

- [1] P.V.R. Schleyer, *J. Am. Chem. Soc.* 79 (1957) 3292.
- [2] D.V. Korolkov, O.V. Sizova, *Int. J. Quantum Chem.* 88 (2002) 606.
- [3] E. Anders, E. Zinner, *Meteorites* 28 (1993) 490.
- [4] L.J. Allamandola, S.A. Sandford, A.G.G.M. Tielens, T.M. Herbst, *Astrophys. J.* 399 (1992) 134.
- [5] O. Guillois, G. Ledoux, C. Renaud, *Astrophys. J.* 521 (1999) L133.
- [6] C. van Kerckhoven, A.G.G.M. Tielens, C. Waelkens, *Astron. Astrophys.* 384 (2002) 568–584.
- [7] H.C. Chang, J.C. Lin, J.Y. Wu, K.H. Chen, *J. Phys. Chem.* 99 (1995) 11081–11088.
- [8] J.C. Blades, D.C.B. Whittet, *Mon. Not. R. Astron. Soc.* 191 (1980) 701.
- [9] W.A. Schutte, A.G.G.M. Tielens, J.L. Allamandola, M. Cohen, D.H. Wooden, *Astrophys. J.* 360 (1990) 577.
- [10] K. Sellgren, *Spectrochim. Acta A* 57 (2001) 627.
- [11] J.E. Dahl, S.G. Liu, R.M.K. Carlson, *Science* 299 (2003) 96.
- [12] J.E.P. Dahl, J.M. Moldowan, T.M. Peakman, J.C. Clardy, E. Lobkovsky, M.M. Olmstead, P.W. May, T.J. Davis, J.W. Steeds, K.E. Peters, A. Pepper, A. Ekuan, R.M.K. Carlson, *Angew. Chem., Int. Ed.* 42 (2003) 2040–2044.
- [13] J. Filik, J.N. Harvey, N.L. Allan, P.W. May, J.E.P. Dahl, S. Liu, R.M.K. Carlson, *Spectrochim. Acta A* 64 (2006) 681–692.
- [14] G. Yan, N.R. Brinkmann, H.F. Schaefer, *J. Phys. Chem. A* 107 (2003) 9479–9485.
- [15] N. Polfer, B.G. Sartakov, J. Oomens, *Chem. Phys. Lett.* 400 (2004) 201–205.
- [16] S.L. Richardson, T. Baruah, M.J. Mehl, M.R. Pederson, *Chem. Phys. Lett.* 403 (2005) 83–88.
- [17] Y.R. Chen, H.C. Chang, C.L. Cheng, C.C. Wang, J.C. Jiang, *J. Chem. Phys.* 119 (2003) 10626–10632.
- [18] A.T. Balaban, P. von Rague Schleyer, *Tetrahedron* 34 (1978) 3599–3609.
- [19] A.D. Becke, *J. Chem. Phys.* 98 (1993) 5648–5652.
- [20] C.W. Bauschlicher, S.R. Langhoff, *Spectrochim. Acta A* 53 (1997) 1225–1240.
- [21] M. J. Frisch et al., Gaussian 98 Revision A.11.4 Gaussian, Inc., Pittsburgh PA.
- [22] A.P. Scott, L. Radom, *J. Phys. Chem.* 100 (1996) 16502–16513.
- [23] <http://webbook.nist.gov>.
- [24] C. Joblin, L. d’Hendecourt, A. Léger, D. Défourneau, *Astron. Astrophys.* 281 (1994) 923–936.